Inorganic Chemistry

Routes to Heterotrinuclear Metal Siloxide Complexes for Cooperative Activation of O$_2$

Marie-Louise Wind, Santina Hoof, Beatrice Braun-Cula, Christian Herwig, and Christian Limberg*

ACCESS | Metrics & More | Article Recommendations | Supporting Information

ABSTRACT: The assembly of heterometallic complexes capable of activating dioxygen is synthetically challenging. Here, we report two different approaches for the preparation of heterometallic superoxide complexes $[^{Ph}L_2Cr^{III}-\eta^1-O_2][MX]_2$ ($^{Ph}L = ^-OPh_2SiOSiPh_2O^-$, MX$^+$ = [CoCl]$^+$, [ZnBr]$^+$, [ZnCl]$^+$) starting from the Cr^{II} precursor complex $[^{Ph}L_2Cr^{II}]Li_2(THF)_4$. The first strategy proceeds via the exchange of Li$^+$ by [MX]$^+$ through the addition of MX$_2$ to $[^{Ph}L_2Cr^{II}]Li_2(THF)_4$ before the reaction with dioxygen, whereas in the second approach a salt metathesis reaction is undertaken after O$_2$ activation by adding MX$_2$ to $[^{Ph}L_2Cr^{III}-\eta^1-O_2]Li_2(THF)_4$. The first strategy is not applicable in the case of redox-active metal ions, such as Fe^{2+} or Co^{2+}, as it leads to the oxidation of the central chromium ion, as exemplified with the isolation of $[^{Ph}L_2Cr^{III}Cl]-[CoCl]_2(THF)_3$. However, it provided access to the hetero-bimetallic complexes $[^{Ph}L_2Cr^{III}-\eta^1-O_2][MX]_2$ ([MX]$^+$ = [ZnBr]$^+$, [ZnCl]$^+$) with redox-inactive flanking metals incorporated. The second strategy can be applied not only for redox-inactive but also for redox-active metal ions and led to the formation of chromium(III) superoxide complexes $[^{Ph}L_2Cr^{III}-\eta^1-O_2][MX]_2$ (MX$^+$ = [ZnCl]$^+$, [ZnBr]$^+$, [CoCl]$^+$). The results of stability and reactivity studies (employing TEMPO−H and phenols as substrates) as well as a comparison with the alkali metal series (M$^+$ = Li$^+$, Na$^+$, K$^+$) confirmed that although the stability is dependent on the Lewis acidity of the counterions M and the number of solvent molecules coordinated to those, the reactivity is strongly dependent on the accessibility of the superoxide moiety. Consequently, replacement of Li$^+$ by XZn$^+$ in the superoxides leads to more stable complexes, which at the same time behave more reactive toward O−H groups. Hence, the approaches presented here broaden the scope of accessible heterometallic O$_2$ activating compounds and provide the basis for further tuning of the reactivity of $[^RL_2Cr^{III}-\eta^1-O_2]M_2$ complexes.
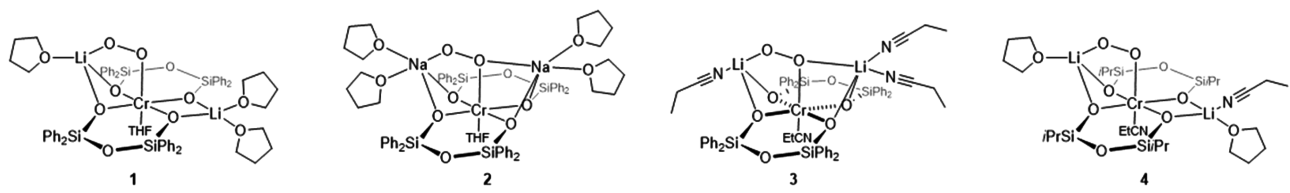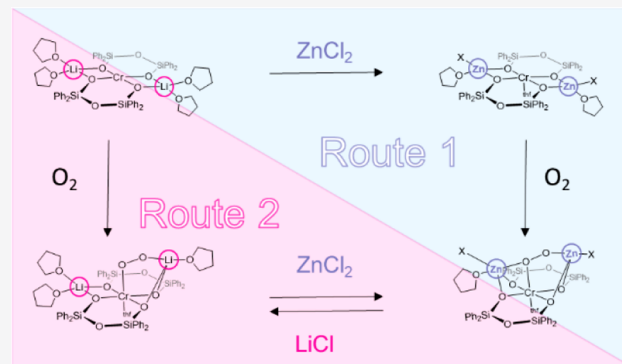
INTRODUCTION

In molecular arrangements the placement of two or more metal centers in close proximity to each other can allow for a communication and/or cooperation between them, for instance, with regard to substrate activation in catalytic cycles.[1−8] In nature the activation of small molecules is often performed by active sites containing several redox-active centers,[9] e.g., the fixation of N$_2$ by nitrogenase[10] or O$_2$ reduction by cytochrome c oxidase.[11] In addition, for biological as well as synthetic systems, it has been shown that properties such as stability and reactivity of multimetallic sites can also be modulated by *redox-inactive* Lewis acidic metal ions. In this context a well-known example for a naturally occurring multimetallic system is the oxygen evolving complex (OEC) in Photosystem II: Four manganese ions are active in the oxidation of water to O$_2$, but the presence of a redox-inactive Lewis acidic Ca^{2+} ion is crucial for proper functioning for reasons not yet entirely understood.[12−15]

To gain more insight into how redox-inert metal ions can cooperate in the activation of small molecules, such as dioxygen, through their Lewis acidic properties, a variety of studies on molecular mono- and dinuclear synthetic systems, capable of reacting with dioxygen or oxygen atom transfer reagents, have been conducted in the recent past.

These studies showed that Lewis acids, added deliberately to reaction solutions, influenced the oxygen reduction rate during the initial step of dioxygen activation.[16] In addition to this, it could be shown, that the presence of a Lewis acid also effects the stability and reactivity of the dioxygen adduct complexes formed.[17−23] In 2017 Nam, Fukuzumi, and co-workers observed a direct correlation between the strength of the Lewis acid employed and the reactivity of an *N*-methylated cyclam iron(III) peroxide complex in electron transfer, nucleophilic, and electrophilic reactions.[24,25] Similar results

Table 1. Spectroscopic and Structural Data of Known Chromium(III) Superoxide Complexes with Siloxide Based Ligand Systems

complex	O−O bond distance/Å	O···M$^+$ distance /Å[a]	UV/vis bands/nm	Raman shift/cm^{-1}	ref
[$^{Ph}L_2Cr$-η^1-O_2]Li$_2$(THF)$_4$ (**1**)	1.334(4)	2.028 3.393	310, 507, 691, 882	–	28
[$^{Ph}L_2Cr$-η^1-O_2]Na$_2$(THF)$_5$ (**2**)	1.334(7), 1.324(7)	2.500/2.562 2.433/2.373	319, 508, 712	–	27
[$^{Ph}L_2Cr$-η^1-O_2]Li$_2$(EtCN)$_4$ (**3**)	1.3126(10)	2.014 3.866	306, 487, 685	1130 ($^{16}O_2$)	27
[$^{iPr}L_2Cr$-η^1-O_2]Li$_2$(THF)$_2$(EtCN)$_4$ (**4**)	1.337	2.014 3.421	309, 489, 693, 927	–	29
[$^{iPr}L_2Cr$-η^1-O_2]Li$_2$(EtCN)$_4$ (**5**)	–	–	309, 489, 693	1123 ($^{16}O_2$)	29

[a]Measured with Mercury 3.10.
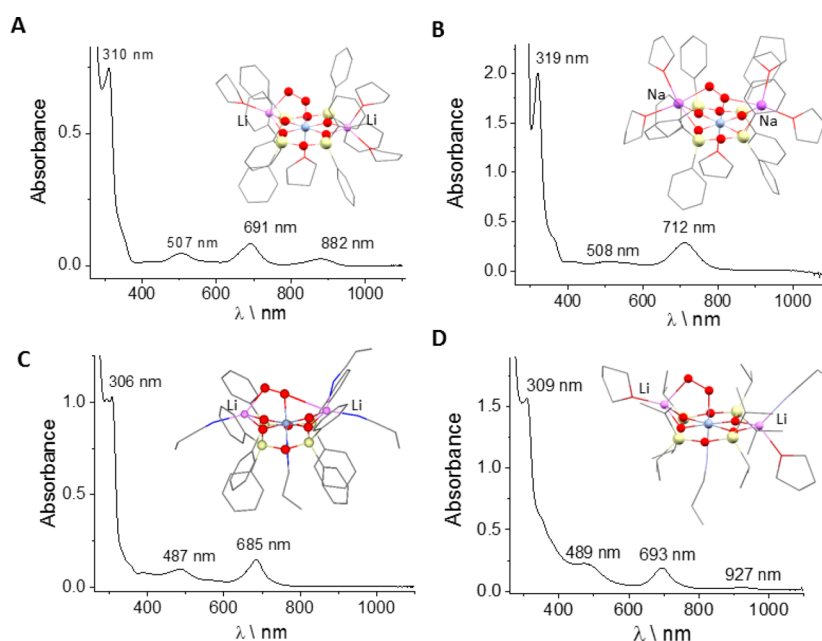
Figure 1. Molecular structures and corresponding UV/vis spectra of previously synthesized chromium(III) superoxide complexes with a siloxide based ligand system. (A) UV/vis spectrum of [$^{Ph}L_2Cr^{III}$-η^1-O_2]Li$_2$(THF)$_4$ (**1**) dissolved in THF. (B) UV/vis spectrum of [$^{Ph}L_2Cr^{III}$-η^1-O_2]Na$_2$(THF)$_5$ (**2**) dissolved in THF. (C) UV/vis spectrum of [$^{Ph}L_2Cr^{III}$-η^1-O_2]Li$_2$(EtCN)$_4$ (**3**) dissolved in EtCN. (D) UV/vis spectrum of [$^{Ph}L_2Cr^{III}$-η^1-O_2]Li$_2$(THF)$_2$(EtCN)$_2$ (**4**) dissolved in a mixture of THF/EtCN. (Data from refs 27−29.)

were rather recently observed for a chromium(III) superoxide complex, but as in case of the iron(III) peroxide Lewis acidic metal ions were added separately to solutions of the already formed dioxygen adduct complex.[26]

We recently investigated a series of chromium(III) superoxide complexes, [$^RL_2Cr^{III}$-η^1-O_2]M$_2$ (L = $^-$OR$_2$SiOSiR$_2$O$^-$) (Table 1), where alkali metal ions (M$^+$ = Li$^+$, Na$^+$, K$^+$) as Lewis acids were an integral part of both, the precursor compounds and the O$_2$ adducts. Their influence and also the effect of the variation of residues R at the siloxane framework (R = Ph, iPr, Me) on the structures, stabilities, and reactivity have been investigated.[27−29]

The superoxide ligands were found to interact with M$^+$ in varying modes (Figure 1 and Table 1). The UV/vis spectra, reactivity, and stability of the superoxide complexes were strongly dependent on these binding modes (M$^+$O$_2$M$^+$ vs M$^+$O$_2$ interaction), the nature of the metal ions M$^+$ (size and Lewis acidity), and the solvent employed (THF and nitriles). Specifically, it could be demonstrated that the stability was mainly influenced by the ionic radius and Lewis acidity of M$^+$, whereas the reactivity of these complexes was not solely dependent on the latter but also on further parameters such as the accessibility of the active center.[27] This shows nicely how versatile the properties of such heterometallic complexes with redox-inactive as well as redox-active metal ions can be, suggesting continuative studies with variation of the flanking metal ions M$^+$.

Scheme 1. Reaction of 6 with Iron(II) Chloride to the Isolated Product [$^{Ph}L_2Cr^{III}Cl$]Li$_2$(THF)$_4$ and with Cobalt(II) Chloride to Give [$^{Ph}L_2Cr^{III}Cl$][CoCl]$_2$(THF)$_3$ (9)
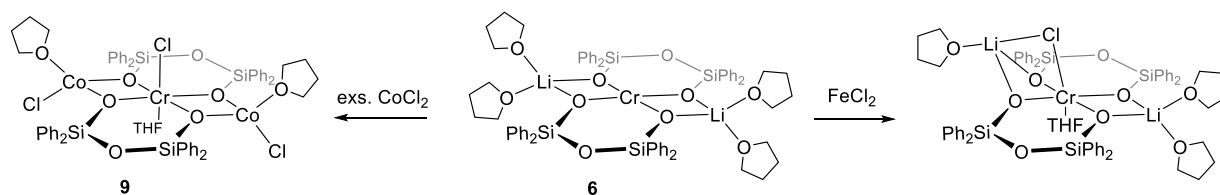
RESULTS AND DISCUSSION

Synthesis of [$^{Ph}L_2Cr^{III}Cl$][CoCl]$_2$(THF)$_3$ (9), [$^{Ph}L_2Cr^{II}$][ZnCl]$_2$(THF)$_3$ (10^{Cl}), and [$^{Ph}L_2Cr^{II}$][ZnBr]$_2$(THF)$_3$ (10^{Br}). We were interested to extend our previous investigations on the cooperative activation of O$_2$ at M/Cr^{II}/M cores from alkali metal ions to transition metal ions. For this purpose the corresponding M/Cr^{II}/M complexes, with M = transition metal ion, had to be prepared.

In general, for the synthesis of complexes of the formula [$^{Ph}L_2M^T$]MM′ (M^T = central transition metal ion; M, M′ = p-block or transition metal ion; $^{Ph}L = ^{-}OPh_2SiOSiPh_2O^{-}$) two different approaches have been employed so far:

(1) In the first method the deprotonation of the disilanol $^{Ph}LH_2$ with different bases MR (R = basic residue), e.g., n-BuLi, LiO^{t}Bu, NaO^{t}Bu, KO^{t}Bu, and KH, is followed by treatment of the resulting $^{Ph}LM_2$ with the transition metal halides. This led to the isolation of heterometallic complexes of the type [$^{Ph}L_2M^T$]M$_2$ (e.g., M = Li$^+$, M^T = Co,[30] Cr,[28,31] Cu;[32,33] M = Na$^+$, M^T = Cr;[34] M = K$^+$, M^T = Cr[27]). However, the suitability of basic compounds with M other than alkali metal ions for the deprotonation step is limited and often does not lead to the formation of the desired product. When, for instance, transition metal amides were used as precursor compounds, homometallic complexes were often isolated.[35]

(2) Sullivan et al.[36] as well as Edelmann and co-workers[37] found that the exposure of [$^{Ph}L_2Co$]Li$_2$(THF)$_4$ to MnCl$_2$ and [$^{Ph}L_2ScCl$]Li$_2$(DME)$_4$ to AlMe$_3$ led to the isolation of crystals of [$^{Ph}L_2Co$]Li(Py$_2$)MnCl(Py) and [$^{Ph}L_2ScCl$]AlMe$_2$Li(THF)$_2$, respectively. In both cases, despite using an excess of reagent, only one of the two counterions could be exchanged without losing the overall structure of the complex.

In our previous research we were able to demonstrate for the series [$^{Ph}L_2Cr^{II}$]M$_2$(THF)$_n$ ($^{Ph}L = ^{-}OPh_2SiOSiPh_2O^{-}$, M$^+$ = Li$^+$, n = 4 (**6**), M$^+$ = Na$^+$, n = 4 (**7**), M$^+$ = K$^+$, n = 2 (**8**)) that varying the size of the alkali metal ions leads to slight changes in the bond distances and angles within the CrO$_4$ plane, which extend to the surroundings of the counterions (Supporting Information, Table S2). Such modifications may explain why in the complex of Edelmann and co-workers only one Li$^+$ could be exchanged by "AlMe$_2$": the difference in ionic radii of four-coordinated Li$^+$ (0.59 Å) and Al^{3+} (0.39 Å)[38,39] leads, in the course of the first substitution, to slight structural changes within the plane inherent to [$^{Ph}L_2ScCl$]Li$_2$(DME)$_4$, which presumably makes the exchange of the second Li$^+$ unfavorable. The same can be assumed for [$^{Ph}L_2Co$]Li(Py$_2$)MnCl(Py) (Mn^{2+}, 0.66 Å). This suggests that an exchange of both Li$^+$ might be achievable, when ions with comparable radii to Li$^+$ are chosen. The ionic radii for four-coordinated iron, cobalt, and zinc complexes with the oxidation state +2 are 0.63, 0.58, and 0.60 Å, respectively; they are thus similar to that of Li$^+$, and hence we decided to test the previously described method (2) to gain access to complexes of the type [$^{Ph}L_2Cr^{II}$][MX]$_2$,

with M = Zn^{2+}, Co^{2+}, Fe^{2+}. For the exchange of Li$^+$ in **6** by [ZnX]$^+$, [FeX]$^+$, and [CoX]$^+$ units (X = Cl$^-$, Br$^-$), ZnCl$_2$, ZnBr$_2$, FeBr$_2$, FeCl$_2$, and CoBr$_2$ as well as CoCl$_2$ were employed as metal precursors.

The reaction of complex **6** with 2.1 equiv of iron(II) chloride led to the isolation of a green solid, which could be identified as the already known complex, [$^{Ph}L_2Cr^{III}Cl$]-Li$_2$(THF)$_4$ (Scheme 1).[27] Hence, the reaction with iron(II) chloride leads to the oxidation of the chromium ion and not to the envisaged complex with Fe^{II} incorporated into the structure.

The reaction of **6** with 2.1 equiv of cobalt(II) chloride led to the formation of a blue solid, which was analyzed by means of ESI-MS, elemental analysis, and IR spectroscopy (see discussion of the spectrum in the Supporting Information (SI)). A single crystal X-ray analysis provided the structure of **9** (Figure 2) and revealed that, again, the central Cr^{II} center had
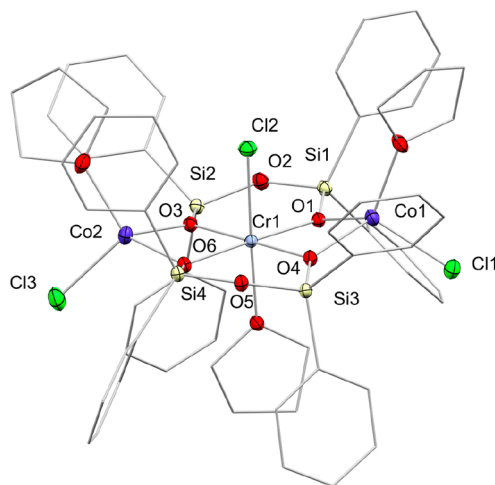
Figure 2. Molecular structure of complex **9** showing 50% probability ellipsoids. For clarity hydrogen atoms as well as noncoordinating solvent molecules are omitted. Selected bond lengths (Å): Co1−O4, 1.9621(18); Co1−O1, 1.9806(18); Co1−Cl1, 2.2334(8); Co1···Cr1, 2.9215(6); Cr1−O4, 1.9691(18); Cr1−O3, 1.9846(18); Cr1−O6, 2.0031(18); Cr1−O1, 2.0036(18); Cr1−Cl2, 2.2969(8); Cr1···Co, 2 2.9506(6); Si1−O1, 1.6308(19); Si1−O2, 1.632(2); Co2−O3, 1.9716(18); Co2−O6, 1.9768(18); Co2−Cl3, 2.2233(8); Si2−O3, 1.6312(19); Si2−O2, 1.6338(19).

been oxidized to Cr^{III} and that both Li$^+$ ions had been exchanged by Co^{2+} ions, thus leading to the product [$^{Ph}L_2Cr^{III}Cl$][CoCl]$_2$(THF)$_3$ (**9**) (see Scheme 1). The terminal chlorido ligand is centered above the square-planar CrO$_4$ unit and does not display any interaction with the cobalt counterions; a THF molecule completes the octahedral coordination sphere of the chromium(III) ion. The chlorido ligands attached to the cobalt counterions are located trans to

the axial chlorido ligand, and the coordination sphere of the cobalt ions is saturated by one THF molecule each.

Although an oxidation of the chromium center has occurred, which makes the resulting complex **9** incapable of activating dioxygen to yield O_2 adducts similar to **1**−**4** (Figure 1), the formation of complex **9** proves that an exchange of both Li^+ counterions via a salt metathesis is possible.

In previous work with β-diketiminato nickel complexes, we have found that replacing a potassium cation interacting with a nickel(II) peroxide unit by a zinc ion leads to a further activation, initiating redox chemistry.[40] Hence, attempts to replace the Li^+ ions in **6** by Zn^{2+} cations suggested itself to gain further insights concerning the influence of the nature of the flanking metal ions in subsequent O_2 activation studies. On the basis of the results obtained in the case of $CoCl_2$ combined with the fact that Zn^{2+} is redox-inert, a clean metathesis reaction was anticipated to result from the treatment of **6** with 2.1 equiv of $ZnCl_2$. After workup, a turquoise powder was isolated, the elemental analysis of which pointed to [$^{Ph}L_2Cr$]-[$ZnCl]_2(THF)_3$ (**10**^{Cl}). ESI-MS measurements of **10**^{Cl} dissolved in THF showed an ion peak at m/z = 1108.8972, which corresponds to [[$^{Ph}L_2Cr$][$ZnCl]_2$+Cl]$^-$ (calcd. m/z = 1108.8961) and corroborates this assignment; the m/z value as well as the isotopic distribution pattern are in good agreement with the calculated values (SI Figure S3). Crystals grown at room temperature from a saturated THF solution were analyzed via X-ray crystallography (Figure 3). The resulting
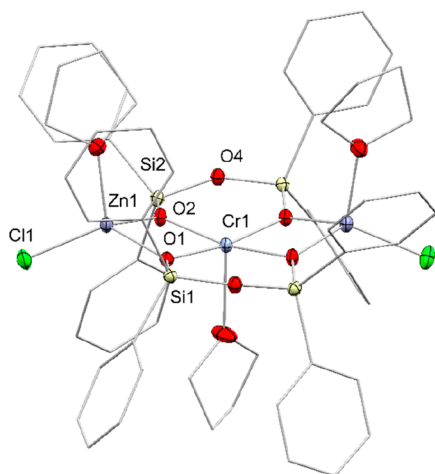

Figure 3. Molecular structure of complex **10**^{Cl} showing 50% probability ellipsoids. For clarity hydrogen atoms as well as noncoordinating solvent molecules are omitted. Selected bond lengths (Å): Cr1−O2, 2.0297(11); Cr1−O1, 2.0338(12); O2−Si2, 1.6180(11); Si2−O4, 1.6291(13); Cr1···Zn1, 2.9587(3); Zn1−Cl1, 2.1779(5); Zn1−O2, 1.9489(12); Zn1−O1, 2.0200(12).

structure shows that indeed both lithium ions have been exchanged and the chromium ion has remained in the oxidation state +2. The Cr^{II} central atom is located in a square-pyramidal coordination sphere composed of two disiloxide ligands, which span the plane, and an additional THF molecule in the apical position. The analogous complex **10**^{Br} can be synthesized and isolated by using $ZnBr_2$ instead of $ZnCl_2$; it was identified as such by X-ray analysis, ESI-MS, and an IR spectrum that closely resembled the one of **10**^{Cl} (SI Figures S1−S3 and Table S2).

Reactivity of [$^{Ph}L_2Cr^{II}$][$ZnCl]_2(THF)_3$ and [$^{Ph}L_2Cr^{II}$][$ZnBr]_2(THF)_3$ toward Dioxygen. The behavior of **10**$^{Cl/Br}$ toward molecular oxygen was tested by exposing a THF solution to dioxygen. ESI-MS measurements performed with the solution showed peaks indicating the formation of a product resulting from a 1:1 reaction with O_2 (SI Figure S4). To gain further insight into what type of O_2 species (e.g., peroxo vs superoxo complex) had been formed, a THF solution of **10**$^{Cl/Br}$ was cooled to 10 °C and exposed to an excess of dioxygen and the reaction was monitored by means of UV/vis spectroscopy. After completion of the reaction, the recorded UV/vis spectrum showed two new distinctive absorption bands at 302 and 675 nm as well as one weak band at 479 nm (Figure 4). A rather similar absorption spectrum was observed for **10**^{Br} upon addition of dioxygen.
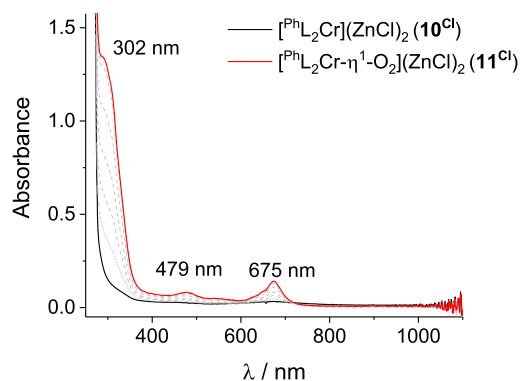

Figure 4. Absorption spectral changes observed during the reaction between **10**^{Cl} and O_2 in THF at 10 °C, leading to the formation of **11**^{Cl}.

In our previous work we had analyzed the band patterns in the UV/vis spectra of chromium(III) superoxide complexes such as **1**−**4** in detail and correlated those to the solid-state structures determined, which were confirmed as relevant also in solution.[27] On the basis of these results we can derive information also concerning the product of the reaction between **10**^{Cl}/**10**^{Br} and dioxygen in THF considering its UV/vis spectrum (Figure 4): Due to the existence of an absorption band at around 300 nm the product can be assigned unambiguously as an *end-on* Cr^{III} superoxo complex (Figure 1 and Table 1).[28,41] The absence of a band in the near-infrared region indicates that *both* of the zinc ions are interacting electrostatically with the oxygen atoms of the superoxide ligand.[27] The comparatively high relative intensity of the band at around 480 nm suggests that the molecule lacks symmetry, most likely caused by different numbers of solvent molecules coordinating to the zinc ions. The band in the 670 nm region implies that in the axial position to the superoxide an additional ligand is attached to the chromium ion, completing an octahedral coordination sphere. Hence, we suggest the formula [$^{Ph}L_2Cr^{III}$-η^1-O_2][$ZnX]_2(THF)_2$ (**11**$^{Br/Cl}$) for the product, with a structure as shown in Scheme 2, similar to the one of **3** (compare UV/vis spectrum in Figure 1). Using propionitrile as the solvent, where **10**$^{Cl/Br}$ is expected[27,29] to convert into [$^{Ph}L_2Cr^{II}$][$ZnX]_2(EtCN)_3$—which for formal distinction we denote separately as *10**$^{Cl/Br}$ (Scheme 2)—an almost identical proceeding as in the case of **10**$^{Cl/Br}$ was observed and bands at 300, 467, and 671 nm were detected for [$^{Ph}L_2Cr^{III}$][$ZnX]_2O_2(EtCN)_2$ (*11**$^{Cl/Br}$), emphasizing that **10**

Scheme 2. Schematic Representation of the Reaction between 6 and ZnX$_2$ (X = Br, Cl) to give 10$^{Cl/Br}$ and *10$^{Cl/Br}$ and Further Reaction with O$_2$ to Yield 11$^{Cl/Br}$ and *11$^{Cl/Br}$, Respectively
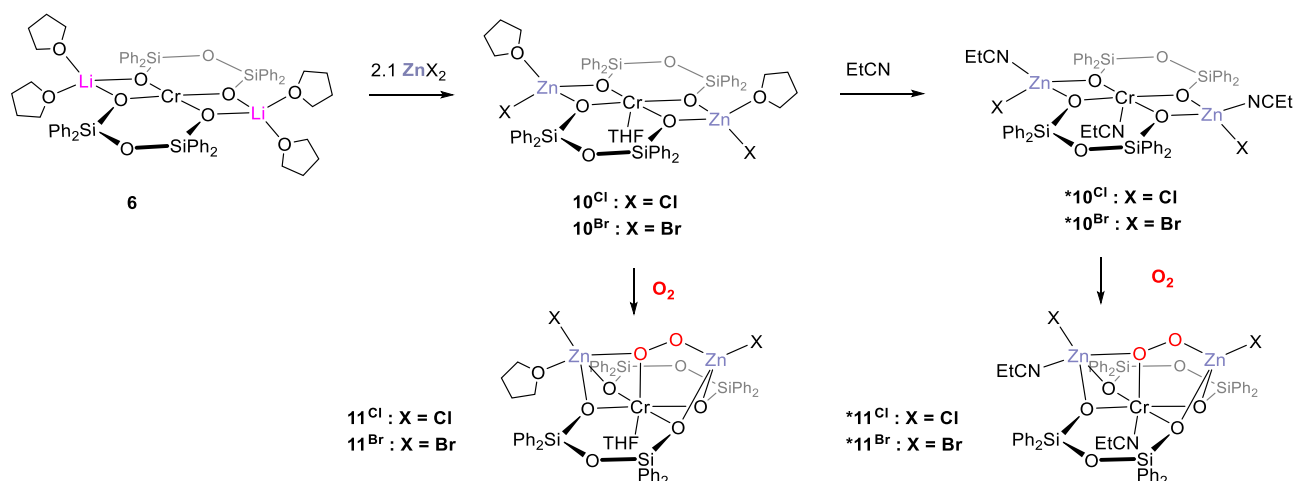
and *10 and correspondingly also 11 and *11 are basically the same core species. Attempts to obtain resonance Raman data remained unsuccessful, despite measuring at different concentrations as well as temperatures and in different solvents.

Stability of [^{Ph}L$_2$Cr^{III}-η^1-O$_2$][ZnCl]$_2$(Sol)$_2$ (Sol = THF (11^{Cl}), EtCN (*11^{Cl})) in THF and EtCN. To gain more insight into how far [ZnX]$^+$ affects the reactivity and stability, self-decay rates of 11^{Cl} and *11^{Cl} were determined. Therefore, 11^{Cl} and *11^{Cl} were generated in THF or EtCN, respectively, and the decay of the bands at 302 nm (THF) or 300 nm (EtCN) as well as the formation of a band typical for the decay product (350 nm) were monitored by UV/vis spectroscopy at 10 °C, respectively (SI Figure S5). First-order rate constants determined for the self-decay of 11^{Cl} revealed that although 11^{Cl} features a M/O$_2$/M interaction similar to that of the Na$^+$ analogue 2 (k_{obs}^{THF} = (5.39 ± 0.02) × 10^{-3} s^{-1}), it exhibits a self-decay rate of k_{obs}^{THF} = (1.11 ± 0.01) × 10^{-4} s^{-1}, which is similar to the one determined for the Li$^+$ analogue 1 (k_{obs}^{THF} = (1.89 ± 0.12) × 10^{-4} s^{-1}) in THF. This may be rationalized first by the fact that zinc ions are more Lewis acidic than sodium ions (and thus lead to more stable Cr–O$_2$···M entities). Moreover, its has been hypothesized and supported previously[27,42] that the self-decay proceeds via the oxidation of the solvent and this could explain the stability of 11^{Cl} additionally: the precoordination of the THF molecules at the flanking metals likely facilitates this process, and while there are four such molecules in the case of 2 and three in 1, there is only one coordinated THF molecule in 11^{Cl}, where chlorido ligands occupy two of the potential binding sites. Hence, 11^{Cl} is even slightly more stable than 1. That the solvent indeed plays a role in the decay reaction could be confirmed: The oxidation products of THF could be detected by means of NMR spectroscopy, and UV/vis spectroscopic monitoring of the decay reaction in deuterated THF revealed a kinetic isotopic effect of KIE = 4.75 (SI Figure S7). Despite many attempts to crystallize 11$^{Cl/Br}$ at −80 °C from THF or EtCN solutions, no crystals suitable for X-ray analysis could be grown. Studying the solvent dependency of the self-decay an observation could be made that further supports the inferences concerning the structures made above: in contrast to [^{Ph}L$_2$Cr^{III}-η^1-O$_2$]Li$_2$(EtCN)$_4$ (3) (k_{obs}^{EtCN} = (4.78 ± 0.30) × 10^{-5} s^{-1}), which is more stable than [^{Ph}L$_2$Cr^{III}-η^1-O$_2$]-Li$_2$(THF)$_4$ (1), likely due to structural changes with regard

to the number of M$^+$/O$_2$ interactions (Li$^+$/O$_2$ in THF vs Li$^+$/O$_2$/Li$^+$ in EtCN) and the CrO$_4$ backbone (planar vs roof-like),[27] the decay rates of 11^{Cl} and *11^{Cl} (k_{obs}^{EtCN} = (1.02 ± 0.05) × 10^{-4} s^{-1}) are almost identical. From this (and on the basis of the comparable bond dissociation energies of THF and EtCN) it can be concluded that the structures are the same in THF and EtCN. Finally, we note that—unlike in the case of the above-mentioned Ni-peroxide-K/Zn system[40]—the zinc ions in the systems investigated here do not lead to a significant increase of superoxide activation compared to alkali metal cations.

Reactivity of [^{Ph}L$_2$Cr^{III}-η^1-O$_2$][ZnCl]$_2$(Sol)$_2$ (Sol = THF (11^{Cl}), EtCN (*11^{Cl})) in THF and EtCN. To assess the reactivity of 11^{Cl} and *11^{Cl}, the decay of their characteristic absorption bands (λ_{THF} = 302 and 675 nm, λ_{EtCN} = 300 and 673 nm) upon addition of 1-hydroxy-2,2,6,6-tetramethylpiperidine (TEMPO–H) was monitored UV/vis spectroscopically. Indeed, the bands disappeared according to a pseudo-first-order rate law and the corresponding rate constants increased proportionally with an increase of the concentration of TEMPO–H, giving second-order rate constants (k_2) of 11.8 ± 1.0 M^{-1} s^{-1} (THF) and 10.4 ± 0.7 M^{-1} s^{-1} (EtCN). The formation of TEMPO was confirmed by means of EPR spectroscopy (SI Figure S9). The second-order rate constants determined for the reactions in THF and EtCN are almost identical within the error margin. This matches the above inferences on the solvent-independent Zn/O$_2$/Zn interactions, and therefore, further experiments were only performed in THF. A comparison of the second-order rate constant of 11^{Cl} with the ones of 1 and 2 shows that 11^{Cl} exhibits a much higher reactivity than 1 (k_2^{THF} = 1.6 ± 0.30 M^{-1} s^{-1}) and 2 (k_2^{THF} = 0.27 ± 0.01 M^{-1} s^{-1}) in THF. In our previous investigations on the alkali metal series we found that the reactivity is determined by two factors, namely, the Lewis acidity of the heterometal and the steric conditions around the superoxide moiety.[27] Decreasing Lewis acidity will lead to more reactive complexes (as the superoxide moiety is less stabilized) but this effect can be overruled by the accessibility of the superoxide function, when structural changes occur with the variation of the metal. The importance of the sterics also in the case of 11^{Cl} became obvious in further investigations performed with phenols as substrates. Compound 11^{Cl} does not react with 2,6-di-*tert*-butylphenol at −80 °C, but it reacts

with 2,6-dimethylphenol (forming 3,3′,5,5′-tetramethyl-4,4′-diphenoquinone), although the bond dissociation energy of the latter is 1.7 kcal/mol higher. A likely reason is the bulkiness of the *tert*-butyl groups, which impede the approach of the substrate. Since the replacement of Li$^+$ by XZn$^+$ was found to lead to more stable complexes, the higher reactivity of **11**^{Cl} compared to **1** and **2**, not only toward substituted phenols but also TEMPO−H, will also have its origin mainly in the higher accessibility of the superoxide unit, which can be rationalized: in the case of **11**^{Cl} two chlorido ligands coordinate to the flanking metal ions instead of solvent molecules, and because the former are less bulky, a more accessible superoxide moiety results, which leads to a higher reactivity.

The findings described above align therefore quite nicely with the observations made so far.

Exchange of Li$^+$ in [^{Ph}L$_2$Cr^{III}-η^1-O$_2$]Li$_2$ (THF)$_4$ (1) by Redox-Active and -Inactive Metal Fragments. Since the exchange of both counterions in the Cr^{II} precursor complexes prior to the reaction with dioxygen (route 1, Scheme 3)

Scheme 3. Formation of 11$^{Cl/Br}$ via 10$^{Cl/Br}$ Prepared from 6 by Treatment with ZnX$_2$ (X = Br, Cl) (Route 1) or through the Reaction of 1 with ZnX$_2$ (Route 2)
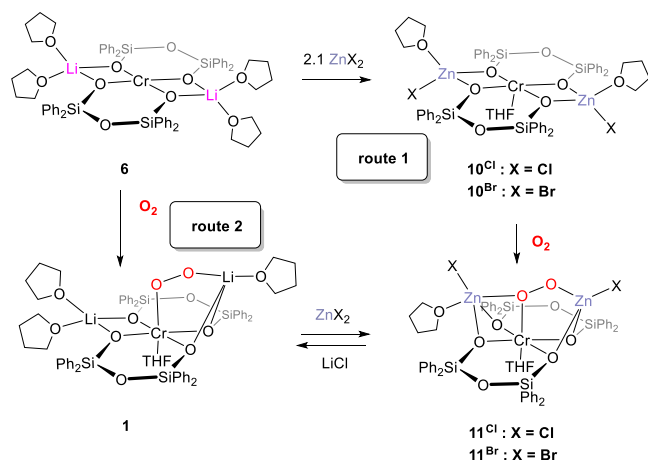
apparently only works for redox-inert transition metal ions (redox-active metal ions employed so far led to the oxidation of the central chromium(II) atom), we contemplated alternative avenues to heterometallic M/Cr(O$_2$)/M complexes, as this would increase the variability of this system. A conceivable synthetic route to such compounds would be a metal exchange with the already formed superoxide complex **1** (route 2, Scheme 3). To test this, we generated **1** in situ at 10 °C in THF and added an excess of ZnCl$_2$ to the solution. The immediate disappearance of the band at 882 nm, which is typical for **1**, and the shift of the other three bands to 302, 479, and 675 nm corroborate the clean conversion of **1** into **11**^{Cl} (SI Figure S10). The exchange reaction can also be performed in the other direction: **1** can be generated by adding an excess of LiCl to a solution of **11**^{Cl} at 10 °C.

Astonishingly these reactions are temperature-controlled and do not take place at low temperatures. Upon applying the same procedure to the reaction of **1** with FeBr$_2$, the immediate disappearance of the band at 882 nm with a simultaneous shift of the band at 310 to 308 nm and a formation of a shoulder at 710 nm indicated an incorporation of Fe^{2+}. Unfortunately, the strong absorption of the newly formed Cr/O$_2$/Fe intermediate

and a subsequent fast oxidation of Fe^{2+} to Fe^{3+} did not allow its further characterization.

However, employing CoCl$_2$ led to the formation of a more stable Co/Cr(O$_2$)/Co superoxide: Upon addition of CoCl$_2$ to a THF solution of **1** the band of **1** at 882 nm disappeared, while simultaneously a shift of the "CoCl" absorption band from 686 to 696 nm occurred (Figure 5).

The band at 696 nm had also been observed for **9** and therefore indicates an incorporation of [CoCl]$^+$ into the structure. The presence of a band at 303 nm, which has shifted from 310 nm (**1**), corroborates the formation of a superoxide species with an end-on bound O$_2$ ligand. Density functional calculations support our assignment as a superoxide (Supporting Information). The band at 696 nm unfortunately masks the usually occurring bands in that region so that more detailed information on the Co/O$_2$ interaction cannot be derived from the UV/vis spectrum. Nevertheless, the obtained results suggest the successful exchange of the counterions and thus the formation of the envisaged complex [^{Ph}L$_2$Cr^{III}-η^1-O$_2$]-[CoCl]$_2$ (**12**). Compound **12** exhibits a self-decay rate of $k_{obs}^{THF} = (7.59 \pm 0.02) \times 10^{-5}$ s^{-1} at 10 °C, which is slightly lower than the rates determined for **1** ($k_{obs}^{THF} = (1.89 \pm 0.12) \times 10^{-4}$ s^{-1}) and **11**^{Cl} ($k_{obs}^{THF} = (1.11 \pm 0.01) \times 10^{-4}$ s^{-1}) in THF. To compare the reactivities of **12** with the reactivity of **11**^{Cl} and the starting compound **1**, the disappearance of the absorption band characteristic of **12** (302 nm) upon addition of TEMPO−H was monitored UV/vis spectroscopically. Pseudo-first-order rate constants determined at −80 °C increased proportionally with an increase of the concentration of TEMPO−H, giving a second-order rate constant (k_2) of $(5.0 \pm 0.2) \times 10^{-3}$ M^{-1} s^{-1} (THF). This very low reactivity is surprising, and at this point we can only assume that either changes in the M$^+$/O$_2$ interaction or the amount of coordinating solvent molecules result in a less accessible superoxide moiety and are therefore responsible for the decreased reactivity.

■ CONCLUSION

We herein present two methods to extend the chemistry of disiloxandiolate based hetero-bimetallic superoxide complexes from chromium/alkali metal to chromium/transition metal combinations. The reaction of **6** with ZnCl$_2$ or ZnBr$_2$ allowed for the isolation of [^{Ph}L$_2$Cr^{II}][ZnX]$_2$(THF)$_2$ (X = Cl, Br), which react with dioxygen forming the Zn/Cr(O$_2$)/Zn superoxide complexes [^{Ph}L$_2$Cr^{III}-η^1-O$_2$][ZnX]$_2$(THF)$_3$ (X = Cl, Br). Similar attempts to prepare corresponding compounds with redox-active ions in place of Zn^{2+} failed due to the oxidation of the Cr^{II} central atom, but we were able to demonstrate for the examples of Zn and Co that the exchange works also at the superoxide level. Since, in the superoxide [^{Ph}L$_2$Cr^{III}-η^1-O$_2$]Li$_2$(THF)$_4$, the Cr center is already in the oxidation state +3, no redox chemistry takes place then in contact with redox-active transition metal ions, so that the salt metathesis to the desired Zn/Cr(O$_2$)/Zn and Co/Cr(O$_2$)/Co compounds can be carried out. Results of the investigation on the reactivity and stability of [^{Ph}L$_2$Cr^{III}-η^1-O$_2$][ZnCl]$_2$(THF)$_2$ confirm that the intrinsic stability is mainly governed by the Lewis acidity of the metal ions and the number of coordinated solvent molecules, whereas the reactivity of such hetero-bimetallic complexes is majorly influenced by the accessibility of the superoxide moiety and, thus, by the structural arrangements around the superoxide moiety; this nicely complements our previous findings. With this information
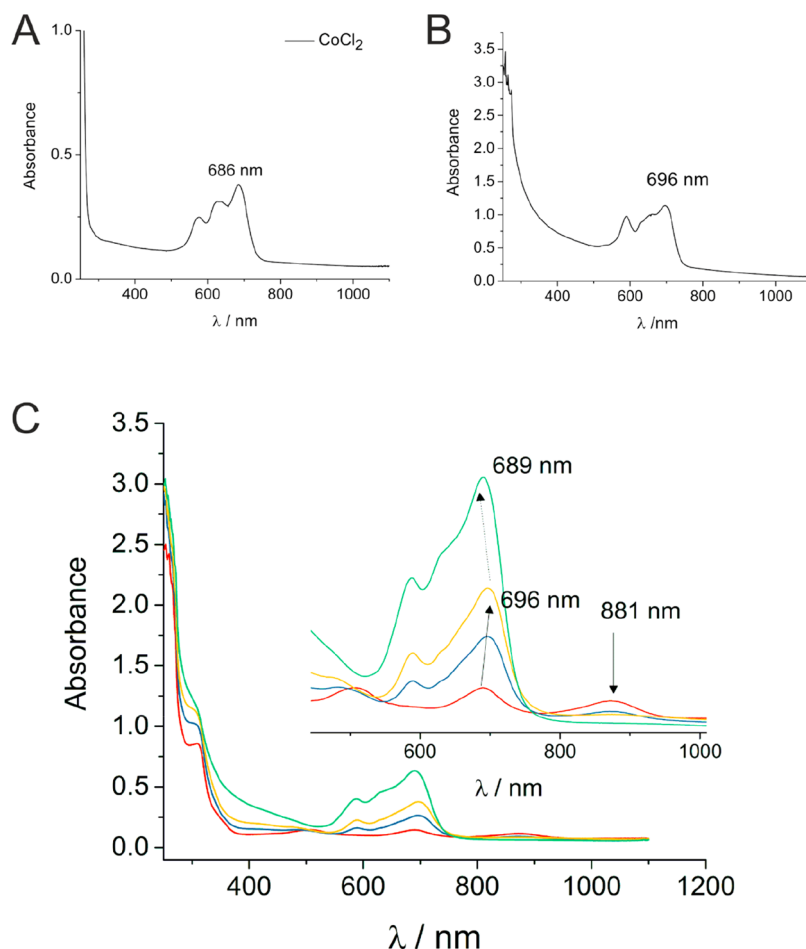
Figure 5. (A) UV/vis spectrum of a THF solution of CoCl$_2$ at 25 °C. (B) UV/vis spectrum of compound **9** at 25 °C for comparison. (C) UV/vis spectral changes observed for a THF solution of **1** upon addition of CoCl$_2$. Red: UV/vis spectrum of **1** before addition of CoCl$_2$. Blue: UV/vis spectrum after addition of a substoichiometric amount of CoCl$_2$. Yellow: UV/vis spectrum after addition of 2.1 equiv of CoCl$_2$. Green: UV/vis spectrum after addition of an excess of CoCl$_2$. Inset shows the band at 696 nm slowly increasing and then shifting to the region of unbound CoCl$_2$ upon addition of an excess of CoCl$_2$. The decrease of the band at 882 nm can also be observed upon addition of CoCl$_2$.

and the methods to create rather different M/Cr(O$_2$)/M cores at hand, we hope to be able to design and control further novel reactive complexes, where two selected metal centers cooperate in O$_2$ activation, in future.

■ EXPERIMENTAL SECTION

General Considerations. All manipulations were carried out in a glovebox, or by means of Schlenk-type techniques involving the use of a dry argon atmosphere. Microanalyses were performed with a Leco CHNS-932 elemental analyzer. Infrared (IR) spectra were recorded with samples prepared as KBr pellets with a Shimadzu FTIR-8400S spectrometer. HR-ESI-MS data were collected using an Agilent Technologies 6210 time-of-flight LC-MS instrument. UV/vis spectra were obtained at variable temperatures using an Agilent 8453 UV–visible spectrophotometer equipped with a Unisoku USP-203-A cryostat. EPR spectra were recorded at an ESR MiniScope MS5000 (Magnettech), equipped with a quartz dewar. Crystal data were collected at a Bruker D8 Venture diffractometer at 100 K, using Mo Kα radiation (λ = 0.71073 Å). The structures were solved by direct methods using SHELXS-97 and refined by full matrix least-squares procedures based on F^2 with all reflections measured with SHELXL-2013.[43,44] Multiscan corrections were applied to the data.[45] All non-hydrogen atoms were refined anisotropically. All hydrogen atom positions were introduced at their idealized positions and were refined using a riding model. CCDC 1949950 (**9**), 1949952 (**10**^{Cl}), and 1949951 (**10**^{Br}) contain the supplementary crystallographic data for

this work. These data can be obtained free of charge from The Cambridge Crystallographic Data Centre via www.ccdc.cam.ac.uk/data_request/cif.

Chemicals. 1,1,3,3-Tetraphenylsilan-1,3-diol was synthesized according to literature.[46] 1,3-Dichloro-1,1,3,3-tetraphenylsiloxane, TEMPO, CoCl$_2$, FeCl$_2$, and CrCl$_2$ were purchased at ABCR and used as received. Compounds **1**, **3**, and **6** were synthesized according to literature,[28] and TEMPO–H was produced according to a previously described modified literature procedure.[27,47] O$_2$ was added via a balloon, which had been thoroughly flushed with argon before being filled with dioxygen.

Solvents. THF was purchased from Acros Organics and was distilled over sodium, degassed, and stored over activated molecular sieves (3 Å) prior to use. Chloroform was dried over CaCl$_2$, refluxed over P$_2$O$_5$, degassed, and stored over activated molecular sieves (4 Å) prior to use. Hexane, diethyl ether, and acetonitrile were dried with an MBraun solvent purification system and degassed prior to use. Propionitrile was purchased from Acros Organics as well as from Sigma-Aldrich, degassed, and stored over activated molecular sieves (3 Å) prior to use.

[^{Ph}L$_2$Cr^{III}Cl][CoCl]$_2$(THF)$_3$ (9). To a solution of **6** (50 mg, 0.04 mmol, 1 equiv) in THF, CoCl$_2$ (11.6 mg, 0.09 mmol, 2.1 equiv) was added, and the solution was stirred overnight at room temperature. The resulting blue solution was filtered and the solvent subsequently removed. The solid residue was washed with hexane, small amounts of Et$_2$O, MeCN, and CHCl$_3$ and redissolved in THF. The solution thus obtained was layered with hexane, which within a few days led to blue

crystals of **9** (17.2 mg, 0.01 mmol, 32%) suitable for single crystal X-ray diffraction analysis. By employing 4 equiv of CoCl$_2$, the yield can be increased to 65%.

Elem. Anal. Found for C$_{60}$H$_{64}$Cl$_3$Co$_2$CrO$_9$Si$_4$: H, 4.53; C, 50.95%. Calcd: H, 4.90; C, 54.69%. Elemental analysis with metal siloxide compounds can lead to low carbon values, even if pure, crystalline material is investigated, likely due to incomplete combustion (SiC formation). In the case of **9** repeated measurements with crystalline and amorphous product led to similar results, where the H content acceptably agrees with the calculated value, while the determined C content is somewhat too low. UV/vis [λ_{max}(THF)/nm (ε/(cm^{-1} mol^{-1} L))]: 590 (93), 660 (95), 696 (105). IR ($\bar{\nu}_{max}$/cm^{-1} (KBr)): 3069 (w), 2976 (w), 2903 (w), 1590 (w), 1429 (m), 1122 (s), 1114 (s), 1041 (s), 1024 (s), 996 (m), 888 (s), 748 (m), 715 (s), 699 (s), 544 (s), 523 (s). HR-ESI-MS. [M − 3THF + H$_2$O + CH$_3$CN]$^-$ (m/z): Calcd for [C$_{50}$H$_{45}$Cl$_3$Co$_2$CrNO$_7$Si$_4$], 1157.9413; found, 1157.9197. [M − 3THF + CH$_2$CH$_2$CN]$^-$ (m/z): Calcd for [C$_{51}$H$_{47}$Cl$_3$Co$_2$CrNO$_6$Si$_4$], 1153.9401; found, 1153.9589.

[^{Ph}L$_2$Cr^{II}][ZnCl]$_2$(THF)$_3$ (**10^{Cl}**). To a solution of **6** (22.0 mg, 0.02 mmol, 1 equiv) in THF, ZnCl$_2$ (5.4 mg, 0.04 mmol, 2.1 equiv) was added, and the solution was stirred overnight at room temperature. The resulting turquoise solution was filtered, and subsequently the solvent was removed under reduced pressure. The solid residue was washed with hexane and small amounts of Et$_2$O and redissolved in THF. The solution thus obtained was layered with hexane, which led within a few days to turquoise crystals of **10^{Cl}** (14.4 mg, 0.01 mmol, 56%), which were suitable for single crystal X-ray diffraction analysis.

Elem. Anal. (of the solid before crystallization). Found for C$_{60}$H$_{64}$Cl$_2$CrO$_9$Si$_4$Zn$_2$: H, 4.83; C, 53.74%. Calcd: H, 4.98; C, 55.64%. (See comments made in the case of **9**.) UV/vis [λ_{max}(THF)/nm (ε/(cm^{-1} mol^{-1} L))]: 672 (28). IR ($\bar{\nu}_{max}$/cm^{-1} (KBr)): 3069 (m), 3045 (m), 2979 (m), 2957 (m), 2882 (m), 1963 (vw), 1893 (vw), 1826 (vw), 1590 (w), 1429 (m), 1123 (s), 1114 (s), 1040 (s), 1023 (s), 996 (s), 893 (s), 744 (m), 717 (s), 700 (s), 553 (s), 526 (w). HR-ESI-MS. [M − 3THF + Cl]$^-$ (m/z): Calcd for [C$_{48}$H$_{40}$Cl$_3$CrO$_6$Si$_4$Zn$_2$]$^-$, 1108.8961; found, 1108.8972.

[^{Ph}L$_2$Cr^{II}][ZnBr]$_2$(THF)$_3$ (**10^{Br}**). To a solution of **6** (22.0 mg, 0.02 mmol, 1 equiv) in THF, ZnBr$_2$ (8.8 mg, 0.04 mmol, 2.1 equiv) was added, and the solution was stirred overnight at room temperature. The turquoise solution was filtered, the solvent removed under reduced pressure, and the solid residue washed with hexane as well as small amounts of Et$_2$O. After redissolving the solid in THF, the solution was layered with hexane, which led to turquoise crystals of **10^{Br}** (15.2 mg, 0.01 mmol, 59%) suitable for single crystal X-ray diffraction analysis.

UV/vis [λ_{max}(THF)/nm (ε/(cm^{-1} mol^{-1} L))]: 672 (28). IR ($\bar{\nu}_{max}$/cm^{-1} (KBr)): 3069 (m), 3045 (m), 2980 (m), 2958 (m), 2885 (m), 1963 (vw), 1893 (vw), 1826 (vw), 1590 (w), 1429 (m), 1124 (s), 1114 (s), 1041 (s), 1024 (s), 995 (m), 887 (s), 743 (m), 718 (s), 699 (s), 554 (s), 524 (w). HR-ESI-MS. [M − 3THF + H$_2$O + MeCN]$^-$ (m/z): Calcd for [C$_{50}$H$_{45}$Br$_2$CrO$_7$NSi$_4$Zn$_2$]$^-$, 1220.8633; found,1220.8484.

[^{Ph}L$_2$Cr-η^1-O$_2$][ZnX]$_2$(Sol)$_2$ (X = Br, Cl; Sol = THF, EtCN) (**11$^{Cl/Br}$** and *****11$^{Cl/Br}$**). Compounds **11$^{Cl/Br}$** and *****11$^{Cl/Br}$** were generated by adding dioxygen to a solution of previously isolated and crystallized **10^{Br}** or **10^{Cl}**, respectively, in the corresponding solvents—dependent on the subsequent investigation—at −80 or 10 °C (route 1). Alternatively, **11$^{Cl/Br}$** can also be accessed by generating [^{Ph}L$_2$Cr-η^1-O$_2$]Li$_2$(THF)$_4$ (**1**) at 10 °C in THF, flushing the solution with argon for 60 s, and then adding 2.1 equiv of either ZnCl$_2$ or ZnBr$_2$ (route 2).

[^{Ph}L$_2$Cr-η^1-O$_2$][CoCl]$_2$. [^{Ph}L$_2$Cr-η^1-O$_2$][CoCl]$_2$ can be obtained by generating **1** in situ, flushing the solution for 60 s with argon, and subsequently adding 2.1 equiv of CoCl$_2$ to the solution at 10 °C (route 2).

ASSOCIATED CONTENT

ⓢ Supporting Information

The Supporting Information is available free of charge at https://pubs.acs.org/doi/10.1021/acs.inorgchem.0c00279.

IR spectra, ESI-MS spectra, crystal structure analysis data, UV/vis spectra, EPR spectra, and density functional calculations (PDF)

Accession Codes

CCDC 1949950−1949952 contain the supplementary crystallographic data for this paper. These data can be obtained free of charge via www.ccdc.cam.ac.uk/data_request/cif, or by emailing data_request@ccdc.cam.ac.uk, or by contacting The Cambridge Crystallographic Data Centre, 12 Union Road, Cambridge CB2 1EZ, UK; fax: +44 1223 336033.

■ AUTHOR INFORMATION

Corresponding Author

Christian Limberg − *Chemistry Department, Humboldt-Universität zu Berlin, 12489 Berlin, Germany;* ◉ orcid.org/0000-0002-0751-1386; Phone: +4930-20937382; Email: Christian.limberg@chemie.hu-berlin.de

Authors

Marie-Louise Wind − *Chemistry Department, Humboldt-Universität zu Berlin, 12489 Berlin, Germany*

Santina Hoof − *Chemistry Department, Humboldt-Universität zu Berlin, 12489 Berlin, Germany*

Beatrice Braun-Cula − *Chemistry Department, Humboldt-Universität zu Berlin, 12489 Berlin, Germany;* ◉ orcid.org/0000-0001-6262-4925

Christian Herwig − *Chemistry Department, Humboldt-Universität zu Berlin, 12489 Berlin, Germany*

Complete contact information is available at:
https://pubs.acs.org/10.1021/acs.inorgchem.0c00279

Notes

The authors declare no competing financial interest.

■ REFERENCES

(1) Buchwalter, P.; Rosé, J.; Braunstein, P. Multimetallic Catalysis Based on Heterometallic Complexes and Clusters. *Chem. Rev.* **2015**, *115* (1), 28−126.

(2) Gavrilova, A. L.; Bosnich, B. Principles of Mononucleating and Binucleating Ligand Design. *Chem. Rev.* **2004**, *104* (2), 349−384.

(3) Bratko, I.; Gómez, M. Polymetallic complexes linked to a single-frame ligand: cooperative effects in catalysis. *Dalton Trans.* **2013**, *42* (30), 10664−10681.

(4) Kure, B.; Sano, M.; Nakajima, T.; Tanase, T. Systematic Heterodinuclear Complexes with MM′(μ-meppp) Centers That Tune the Properties of a Nesting Hydride (M = Ni, Pd, Pt; M′ = Rh, Ir; H$_2$meppp = meso-1,3-Bis[(mercaptoethyl)phenylphosphino]-propane). *Organometallics* **2014**, *33* (15), 3950−3965.

(5) Park, J.; Hong, S. Cooperative bimetallic catalysis in asymmetric transformations. *Chem. Soc. Rev.* **2012**, *41* (21), 6931−6943.

(6) Shibasaki, M.; Yoshikawa, N. Lanthanide Complexes in Multifunctional Asymmetric Catalysis. *Chem. Rev.* **2002**, *102* (6), 2187−2210.

(7) Lang, P.; Schwalbe, M. Pacman Compounds: From Energy Transfer to Cooperative Catalysis. *Chem. - Eur. J.* **2017**, *23* (69), 17398−17412.

(8) Mankad, N. P. Selectivity Effects in Bimetallic Catalysis. *Chem. - Eur. J.* **2016**, *22* (17), 5822−5829.

(9) Karlin, K. Metalloenzymes, structural motifs, and inorganic models. *Science* **1993**, *261* (5122), 701−708.

(10) Howard, J. B.; Rees, D. C. How many metals does it take to fix N_2? A mechanistic overview of biological nitrogen fixation. *Proc. Natl. Acad. Sci. U. S. A.* **2006**, *103* (46), 17088−17093.

(11) Schultz, B. E.; Chan, S. I. Structures and Proton-Pumping Strategies of Mitochondrial Respiratory Enzymes. *Annu. Rev. Biophys. Biomol. Struct.* **2001**, *30* (1), 23−65.

(12) Koua, F. H. M.; Umena, Y.; Kawakami, K.; Shen, J.-R. Structure of Sr-substituted photosystem II at 2.1 Å resolution and its implications in the mechanism of water oxidation. *Proc. Natl. Acad. Sci. U. S. A.* **2013**, *110* (10), 3889−3894.

(13) Lohmiller, T.; Shelby, M. L.; Long, X.; Yachandra, V. K.; Yano, J. Removal of Ca^{2+} from the Oxygen-Evolving Complex in Photosystem II Has Minimal Effect on the Mn_4O_5 Core Structure: A Polarized Mn X-ray Absorption Spectroscopy Study. *J. Phys. Chem. B* **2015**, *119* (43), 13742−13754.

(14) Taguchi, Y.; Noguchi, T. Drastic changes in the ligand structure of the oxygen-evolving Mn cluster upon Ca^{2+} depletion as revealed by FTIR difference spectroscopy. *Biochim. Biophys. Acta, Bioenerg.* **2007**, *1767* (6), 535−540.

(15) Vrettos, J. S.; Stone, D. A.; Brudvig, G. W. Quantifying the Ion Selectivity of the Ca^{2+} Site in Photosystem II: Evidence for Direct Involvement of Ca^{2+} in O_2 Formation. *Biochemistry* **2001**, *40* (26), 7937−7945.

(16) Ohkubo, K.; Menon, S. C.; Orita, A.; Otera, J.; Fukuzumi, S. Quantitative Evaluation of Lewis Acidity of Metal Ions with Different Ligands and Counterions in Relation to the Promoting Effects of Lewis Acids on Electron Transfer Reduction of Oxygen. *J. Org. Chem.* **2003**, *68* (12), 4720−4726.

(17) Chen, J.; Lee, Y.-M.; Davis, K. M.; Wu, X.; Seo, M. S.; Cho, K.-B.; Yoon, H.; Park, Y. J.; Fukuzumi, S.; Pushkar, Y. N.; Nam, W. A Mononuclear Non-Heme Manganese(IV)−Oxo Complex Binding Redox-Inactive Metal Ions. *J. Am. Chem. Soc.* **2013**, *135* (17), 6388−6391.

(18) Lacy, D. C.; Park, Y. J.; Ziller, J. W.; Yano, J.; Borovik, A. S. Assembly and Properties of Heterobimetallic $Co^{II/III}/Ca^{II}$ Complexes with Aquo and Hydroxo Ligands. *J. Am. Chem. Soc.* **2012**, *134* (42), 17526−17535.

(19) Leeladee, P.; Baglia, R. A.; Prokop, K. A.; Latifi, R.; de Visser, S. P.; Goldberg, D. P. Valence Tautomerism in a High-Valent Manganese−Oxo Porphyrinoid Complex Induced by a Lewis Acid. *J. Am. Chem. Soc.* **2012**, *134* (25), 10397−10400.

(20) Park, Y. J.; Cook, S. A.; Sickerman, N. S.; Sano, Y.; Ziller, J. W.; Borovik, A. S. Heterobimetallic complexes with M^{III}-$(\mu$-OH$)$-M^{II} cores (M^{III} = Fe, Mn, Ga; M^{II} = Ca, Sr, and Ba): structural, kinetic, and redox properties. *Chem. Sci.* **2013**, *4* (2), 717−726.

(21) Park, Y. J.; Ziller, J. W.; Borovik, A. S. The Effects of Redox-Inactive Metal Ions on the Activation of Dioxygen: Isolation and Characterization of a Heterobimetallic Complex Containing a Mn^{III}−$(\mu$-OH$)$−Ca^{II} Core. *J. Am. Chem. Soc.* **2011**, *133* (24), 9258−9261.

(22) Yoon, H.; Lee, Y.-M.; Wu, X.; Cho, K.-B.; Sarangi, R.; Nam, W.; Fukuzumi, S. Enhanced Electron-Transfer Reactivity of Nonheme Manganese(IV)−Oxo Complexes by Binding Scandium Ions. *J. Am. Chem. Soc.* **2013**, *135* (24), 9186−9194.

(23) Zwettler, N.; Walg, S. P.; Belaj, F.; Mösch-Zanetti, N. C. Heterolytic Si−H Bond Cleavage at a Molybdenum-Oxido-Based Lewis Pair. *Chem. - Eur. J.* **2018**, *24* (28), 7149−7160.

(24) Bae, S. H.; Lee, Y.-M.; Fukuzumi, S.; Nam, W. Fine Control of the Redox Reactivity of a Nonheme Iron(III)−Peroxo Complex by Binding Redox-Inactive Metal Ions. *Angew. Chem., Int. Ed.* **2017**, *56* (3), 801−805.

(25) Bang, S.; Lee, Y.-M.; Hong, S.; Cho, K.-B.; Nishida, Y.; Seo, M. S.; Sarangi, R.; Fukuzumi, S.; Nam, W. Redox-inactive metal ions modulate the reactivity and oxygen release of mononuclear non-haem iron(III)−peroxo complexes. *Nat. Chem.* **2014**, *6*, 934.

(26) Devi, T.; Lee, Y.-M.; Nam, W.; Fukuzumi, S. Tuning Electron-Transfer Reactivity of a Chromium(III)−Superoxo Complex Enabled

by Calcium Ion and Other Redox-Inactive Metal Ions. *J. Am. Chem. Soc.* **2020**, *142* (1), 365−372.

(27) Wind, M.-L.; Hoof, S.; Herwig, C.; Braun-Cula, B.; Limberg, C. The Influence of Alkali Metal Ions on the Stability and Reactivity of Chromium(III) Superoxide Moieties Spanned by Siloxide Ligands. *Chem. - Eur. J.* **2019**, *25* (22), 5743−5750.

(28) Schax, F.; Suhr, S.; Bill, E.; Braun, B.; Herwig, C.; Limberg, C. A Heterobimetallic Superoxide Complex formed through O_2 Activation between Chromium(II) and a Lithium Cation. *Angew. Chem., Int. Ed.* **2015**, *54* (4), 1352−1356.

(29) Wind, M.-L.; Hoof, S.; Braun-Cula, B.; Herwig, C.; Limberg, C. Switching from a Chromium(IV) Peroxide to a Chromium(III) Superoxide upon Coordination of a Donor in the trans Position. *J. Am. Chem. Soc.* **2019**, *141* (36), 14068−14072.

(30) Hursthouse, M. B.; Mazid, M. A.; Motevalli, M.; Sanganee, M.; Sullivan, A. C. Cyclic cobaltadisiloxane compounds. Crystal structures of a pyridinolithium [bis(cyclosiloxy)cobalt] cobalt chloride and a bis(tetramethylethylenediaminolithium)-bis(cyclosiloxy)cobaltate. *J. Organomet. Chem.* **1990**, *381* (2), C43−C46.

(31) Abrahams, I.; Lazell, M.; Motevalli, M.; Simon, C. K.; Sullivan, A. C. Structurally different divalent metallasiloxanes [Mg{O-$(Ph_2SiO)_2$}$_2$]-μ-(LiPy)-μ-{(LiPy)$_3$(OH)(Cl)}], [Cr{O$(Ph_2SiO)_2$}$_2$-μ-$(LiPy)_2$$_2$], and [{O$(Ph_2SiO)_2$}$_2$Co{O$(Ph_2SiO)_3$)}-$\mu$-$(LiPy_2)_2$] from $Ph_2Si(OH)_2$/2BuLi and the metal dichlorides. *Chem. Heterocycl. Compd. (N. Y., NY, U. S.)* **1999**, *35* (8), 954−964.

(32) Evans, W. J.; Broomhall-dillard, R. N. R.; Simon, D.; Ziller, J. W. Synthesis and X-ray crystal structure of the dilithium copper siloxide Cu(μ-OSiPh$_2$OSiPh$_2$O)$_2$ [Li(THF)$_2$]$_2$. *J. Coord. Chem.* **1999**, *46* (3), 347−354.

(33) Hursthouse, M. B.; Motevalli, M.; Sanganee, M.; Sullivan, A. C. Exchange of cobalt(II) for copper(II) in a spirocyclic metallasiloxane compound; X-ray crystal structure of the spirocyclic copper(II)-siloxane Cu(OSiPh$_2$OSiPh$_2$O)$_2$-μ-(Lipy)$_2$(py = pyridine). *J. Chem. Soc., Chem. Commun.* **1991**, No. 24, 1709−1710.

(34) Motevalli, M.; Sanganee, M.; Savage, P. D.; Shah, S.; Sullivan, A. C. Synthesis, crystal structure and homogeneous catalytic activity towards ethylene polymerisation of the spirocyclic chromium(II) siloxane [[Cr{(OSiPh$_2$OSiPh$_2$)-μ-Na(thf)$_2$}$_2$](thf = tetrahydrofuran). *J. Chem. Soc., Chem. Commun.* **1993**, No. 14, 1132−1133.

(35) Gosink, H.-J.; Roesky, H. W.; Schmidt, H.-G.; Noltemeyer, M.; Irmer, E.; Herbst-Irmer, R. Synthesis and Structures of Cyclic and Acyclic Metallasiloxanes of Groups 5−7. *Organometallics* **1994**, *13* (9), 3420−3426.

(36) Abrahams, I.; Motevalli, M.; Shah, D.; Sullivan, A. C.; Thornton, P. Mixed metal spirocyclic metallasiloxanes. Crystal structure of the pyridinolithium{bis(cyclodisiloxanediolato)bis-(pyridino)cobalt}pyridinomanganese chloride compound [(Py$_2$Li)-μ-{(Co(OSiPh$_2$OSiPh$_2$O)$_2$·2Py}-μ-MnClPy]. *J. Chem. Soc., Chem. Commun.* **1993**, *0* (19), 1514−1515.

(37) Giessmann, S.; Blaurock, S.; Lorenz, V.; Edelmann, F. T. Unusual Inorganic Ring Systems of Scandium and Yttrium Containing Group 13 Metals: Coordination of Monomeric Me$_2$InOMe to Yttrium. *Inorg. Chem.* **2007**, *46* (26), 10956−10958.

(38) Shannon, R. Revised effective ionic radii and systematic studies of interatomic distances in halides and chalcogenides. *Acta Crystallogr., Sect. A: Cryst. Phys., Diffr., Theor. Gen. Crystallogr.* **1976**, *32* (5), 751−767.

(39) Brown, I. D.; Skowron, A. Electronegativity and Lewis acid strength. *J. Am. Chem. Soc.* **1990**, *112* (9), 3401−3403.

(40) Yao, S.; Xiong, Y.; Vogt, M.; Grützmacher, H.; Herwig, C.; Limberg, C.; Driess, M. O-O Bond Activation in Heterobimetallic Peroxides: Synthesis of the Peroxide [LNi($\mu,\eta^2{:}\eta^2$-O$_2$)K] and its Conversion into a Bis(μ-Hydroxo) Nickel Zinc Complex. *Angew. Chem.* **2009**, *121* (43), 8251−8254.

(41) Cho, J.; Woo, J.; Nam, W. An "End-On" Chromium(III)-Superoxo Complex: Crystallographic and Spectroscopic Character-ization and Reactivity in C−H Bond Activation of Hydrocarbons. *J. Am. Chem. Soc.* **2010**, *132* (17), 5958−5959.

I

(42) Qin, K.; Incarvito, C. D.; Rheingold, A. L.; Theopold, K. H. A Structurally Characterized Chromium(III) Superoxide Complex Features "Side-on" Bonding. *Angew. Chem., Int. Ed.* **2002**, *41* (13), 2333−2335.

(43) Sheldrick, G. A short history of SHELX. *Acta Crystallogr., Sect. A: Found. Crystallogr.* **2008**, *64* (1), 112−122.

(44) Sheldrick, G. Crystal structure refinement with SHELXL. *Acta Crystallogr., Sect. C: Struct. Chem.* **2015**, *71* (1), 3−8.

(45) Sheldrick, G. *SADABS, Software for Empirical Absorption Corrections*; University of Göttingen, 1996.

(46) Seki, H.; Abe, Y.; Gunji, T. Stereochemistry of the reaction of cis,trans,cis-2,4,6,8-tetraisocyanato-2,4,6,8-tetramethylcyclotetrasiloxane with triphenylsilanol and 1,1,3,3-tetraphenyldisiloxane-1,3-diol. *J. Organomet. Chem.* **2011**, *696* (4), 846−851.

(47) Mader, E. A.; Larsen, A. S.; Mayer, J. M. Hydrogen Atom Transfer from Iron(II)−Tris[2,2'-bi(tetrahydropyrimidine)] to TEMPO: A Negative Enthalpy of Activation Predicted by the Marcus Equation. *J. Am. Chem. Soc.* **2004**, *126* (26), 8066−8067.